Aberration-corrected STEM–EELS studies of precipitates in an Al–Mg–Si–Cu–Ag alloy

Sigurd Wenner[a], Calin D. Marioara[b], Quentin M. Ramasse[c], Despoina-Maria Kepaptsoglou[c], Fredrik S. Hage[c], Randi Holmestad[a]

[a] *Department of Physics, NTNU, Høgskoleringen 5, Trondheim NO-7491, Norway*
[b] *Materials and Chemistry, SINTEF, Høgskoleringen 5, Trondheim NO-7491, Norway*
[c] *SuperSTEM Laboratory, STFC Daresbury Campus, Keckwick Lane, Daresbury WA4 4AD, United Kingdom*

Abstract

Aberration corrected scanning transmission electron microscopy combined with electron energy loss spectroscopy has been used to determine the distribution of Cu and Ag atomic columns of precipitates in an Al–Mg–Si–Cu–Ag alloy. Cu columns were commonly part of C and Q′ phases, with the atomic columns having large projected separations. Columns containing Ag were more tightly spaced, in areas lacking repeating unit cells and at incoherent precipitate–host lattice interfaces. Cu-rich and Ag-rich areas were not found to intermix.

Keywords: Aluminium alloys, Precipitation, Scanning transmission electron microscopy, Electron energy loss spectroscopy

Al–Mg–Si alloys are heat-treatable and gain a significant strength increase upon nucleation and growth of hardening nano-sized metastable phases. Detailed investigations of the precipitation sequence have been performed over the years, and crystal structures of most metastable phases have been solved by means of quantitative transmission electron microscopy (TEM) combined with first-principles calculations [1, 2]. When Cu is addded to the alloys, the precipitate phases of the Al–Mg–Si system are suppressed [3], and new, Cu-containing phases such as C [4] and Q' [5, 6, 7] form. Additionally, areas with no repeating unit cell become more common in the structure of the precipitates. Characteristic for all metastable precipitates in the Al–Mg–Si(–Cu)

Email address: sigurd.wenner@ntnu.no (Sigurd Wenner)

system is that they have one main coherency (and growth) direction, along $\langle 001 \rangle_{\mathrm{Al}}$. Consequently, they all are needle-, lath- or plate-shaped. Moreover, they contain a common network of Si columns along their main growth direction, with a projected near-hexagonal structure [8]. Atomic columns of Mg, Al and Cu occupy positions in-between these Si columns, all three having different preferred local atomic configurations and site symmetries. Small additions of Cu to Al–Mg–Si alloys have been found to increase the mechanical strength [3], and additions of Ag have a similar effect [9]. The reason for this is that Cu and Ag promote precipitate nucleation, and create a microstructure of smaller precipitates with higher number density. Recent work has shown that Ag enters the (Cu-free) β' precipitate and replaces 1/3 of its Si atomic columns, creating its own local symmetries [10]. In this paper we reveal the different roles played by Cu and Ag atoms in metastable precipitates in Al–Mg–Si–Cu–Ag alloys.

High-angle annular dark-field scanning TEM (HAADF–STEM) has proven to be a very useful technique for investigating the structure of precipitates in Al alloys. This is due to the properties of high-angle scattered electrons: they are incoherent and form an easily interpretable image, as the contrast is generally unaffected by small changes in objective lens defocus and specimen thickness [11, 12, 13]. In addition, the scattered intensity (Rutherford and thermal diffuse scattering) from an atomic column increases with its atomic number Z. The development of C_{s} aberration correctors [14, 15] has improved the technique by achieving spatial resolutions below 0.1 nm. These attributes make the identification of pure Cu ($Z = 29$) and Ag ($Z = 47$) atomic columns straightforward, and even enables the distinction of Si ($Z = 14$) from Al ($Z = 13$) and Mg ($Z = 12$) columns [10]. However, the technique has certain limitations: elements close in Z (such as Al and Mg), mixed atomic columns, and columns with partial occupancies make it difficult to form atomic models of entire precipitates. On the other hand, electron energy loss spectroscopy (EELS) does not suffer from the mentioned limitations. This TEM technique is commonly used for extracting compositional information and properties of the electronic structure from nano-sized regions in materials. The combination of EELS and aberration-corrected STEM has been successfully used for atomic resolution elemental mapping and electronic fine structure studies in e.g. metal oxides [16, 17]. There has been few attempts to copy this success to the case of aluminium alloys. Al and its neighbours in the periodic table are not particularly suitable for EELS analysis because their L-edges overlap with the Al plasmon peaks, and their K-edges are of high energy and

Table 1: Nominal composition of the studied alloy (at.%).

Mg	Si	Mn	Fe	Cu	Ag	Al
1.00	0.62	0.27	0.10	0.14	0.03	Balance

will thus give poor statistics. However, recent advances such as dual energy range EELS [18] will make the Al-K, Mg-K and Si-K edges more available for analysis.

In this work metastable precipitates formed in an Al–Mg–Si–Cu–Ag alloy have been imaged by probe C_s corrected HAADF–STEM and the distribution of Ag and Cu atomic columns has been analyzed with atomic resolution EELS elemental mapping. These two elements were chosen since their edges Ag-$M_{4,5}$ at 367 eV and Cu-$L_{2,3}$ at 931 eV, combined with their high HAADF–STEM Z contrast, make them suitable for detailed analysis. This model system is thus used to emphasize the advantages of atomic-resolution EELS for precipitate structure determination.

The composition of the extruded profiles used in the study is given in Table 1. The elements Mn and Fe were added to form dispersoid particles that reduce the grain size of the material, and do not participate in precipitation of hardening phases. To achieve an over-aged microstructure composed of finely dispersed Cu-containing precipitates, the following heat treatment was applied: 30 minutes of solution heat treatment at 530 °C, quenching in water and storage for 4 hours at room temperature, aging to peak hardness with 12 hours of annealing at 155 °C and lastly over-aging for 21 days at 200 °C. The TEM specimen was prepared by mechanical polishing, dimpling and ion milling with energies from 4.0 keV down to 1.5 keV. To prevent carbon contamination, the specimen was baked in vacuum at approx. 135 °C for 6 hours before loading in the microscope, and was given regular electron beam showers during microscopy. Tests were performed to ensure that the baking procedure does not alter the microstructure significantly.

HAADF–STEM and EELS spectrum imaging were performed using an aberration corrected Nion UltraSTEM™ 100 at the SuperSTEM facility in Daresbury, UK. Its cold FEG electron source gives a native energy resolution of 0.35 eV, and the minimum expected probe size is 0.08 nm. A voltage of 100 kV was applied. The beam convergence angle was 30 mrad, the HAADF–STEM detector angles were 74–185 mrad and the EELS collection angle was 31 mrad. A dispersion of 1.0 eV/channel was always used.

EEL spectra were acquired in the energy loss range 280–1620 eV. This includes the edges Ag-$M_{4,5}$ at 367 eV, Cu-$L_{2,3}$ at 931 eV and Mg-K at 1305 eV, but does not make any Al or Si edges available. The spectra were improved by means of principal component analysis (PCA) using the software HyperSpy (previously EELSLab [19]). Consequently, the spectrum images were improved to the point that some atomic columns of Ag could be resolved, despite a very noisy starting point. The elemental maps were created in Gatan DigitalMicrograph by manual integration of EELS edges after power-law background subtraction.

The investigated specimen had a high number density of hardening precipitates, most of them plate-/lath-shaped. Two examples of such precipitates are given in Figs. 1 and 3. All observed particles contained both Cu and Ag, and had some regions with no repeating unit cells, although structural units of the Q' and C phases [marked with connected lines on Figs. 1(b) and 3(b)] were a common occurence. The summed EEL spectrum from the full area of Fig. 1 is shown in Fig. 2. For both precipitates, clear Cu-L and Mg-K edges could be seen in the spectra, while the low total content of Ag makes the Ag-M edge barely visible. Due to the small probe size and the long acquisition time required for EELS, beam damage was observed in some datasets. The HAADF–STEM images from the two sets chosen for the present analysis revealed little to no damage.

There is a very good correspondence between bright spots in the HAADF-STEM images and those in the Cu maps, for both precipitates. This enabled identification of most Cu atomic columns. The precipitate in Fig. 1 has two areas where Cu columns form a Q′ configuration, shown with connected lines. Most of the other Cu columns are located along coherent precipitate interfaces and are not related to any periodic structure. All Cu columns in Fig. 3 form a C phase configuration, making the two figures representative of two types of precipitates observed in the specimen.

As opposed to the Cu maps, the Ag maps indicate a broader distribution, over many neighboring atomic columns and in compact areas, for both precipitates. Delocalization of M edges is a known issue [20], which can give an apparent intensity spread to neighboring columns. We see however certain clearly resolved Ag-containing columns quite close to each other in Fig. 3(d), with corresponding bright spots in the HAADF–STEM images [Fig. 3(b)]. A variable Z contrast, and one merely comparable to that of Cu, indicates that Ag is mixed with other, lighter elements in its atomic columns. It is interesting that Ag-rich areas do not overlap with Cu atomic columns, with some

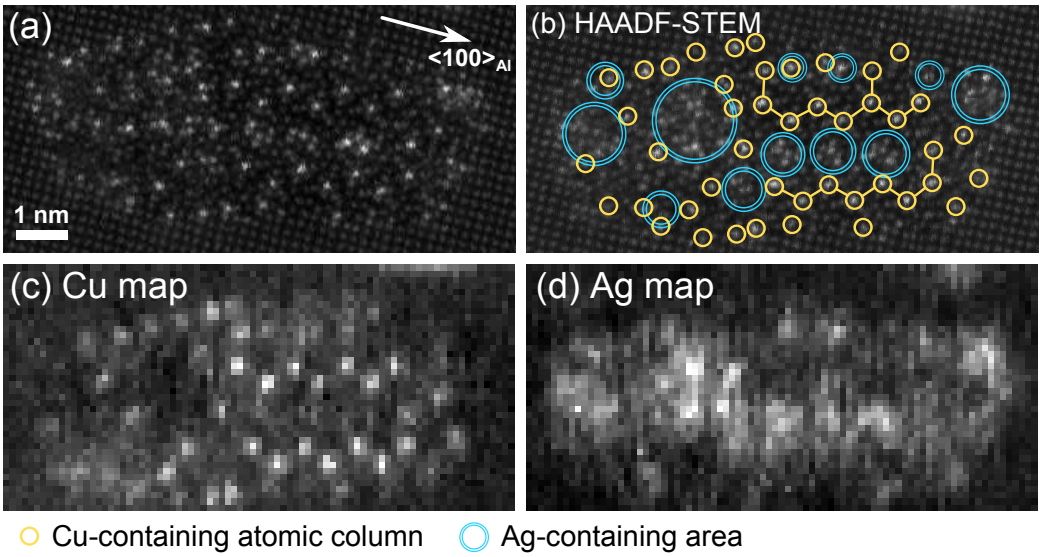

Figure 1: Raw HAADF–STEM images of a precipitate cross-section (a,b), taken respectively before and during the STEM–EELS acquisition. Images (c,d) show EELS elemental maps of Cu and Ag. The location of Cu atomic columns and areas rich in Ag are marked in (b). Cu columns in a Q′ configuration are connected by lines.

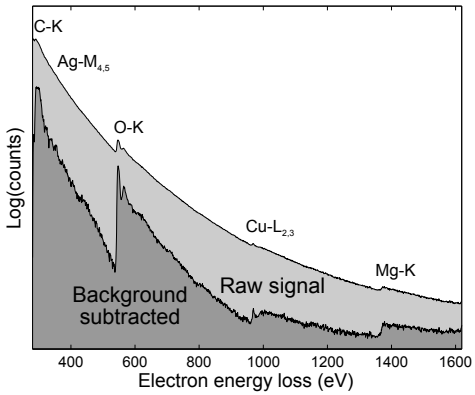

Figure 2: Accumulated EEL spectrum of the area in Fig. 1, in the energy loss range 280–1620 eV. Note the logarithmic intensity axis. The lower curve is background subtracted (global power-law background) and scaled up for easier identification of the edges. The Ag-$M_{4,5}$ edge is still difficult to observe as it is blocked out by the C-K fine structure.

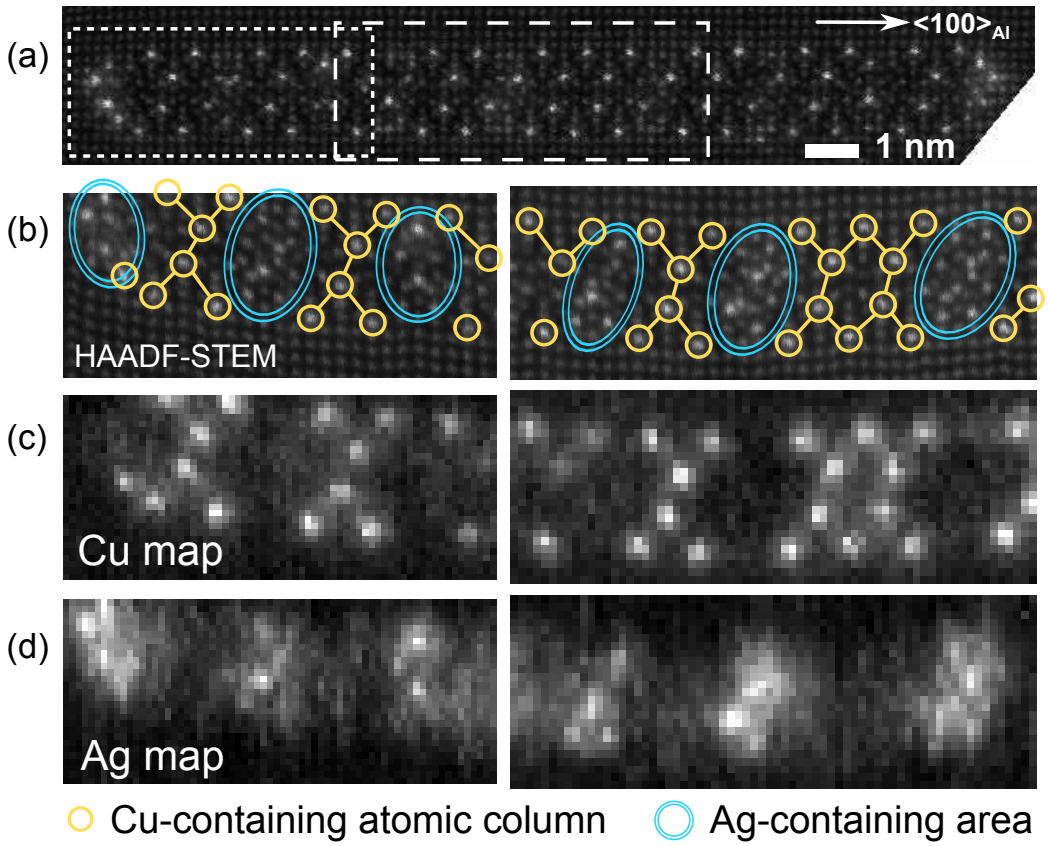

Figure 3: Raw HAADF–STEM images of a precipitate cross-section (a,b), taken respectively before and during the STEM–EELS acquisition. EELS elemental maps of Cu and Ag from the two acquisition areas marked in (a) are shown in (c,d). The skew in the images are caused by specimen drift. The location of Cu atomic columns and areas rich in Ag are marked in (b). Cu columns in a C configuration are connected by lines.

exceptions in Fig. 1. Different preferred configurations of neighboring atoms might explain the lack of mixed Ag/Cu columns in these precipitates. Ag seems to be interupting the formation of ordered Al–Mg–Si–Cu precipitates, and instead creating Ag-rich areas with no repeating unit cells. Accumulations of Ag were commonly observed at incoherent precipitate–host lattice interfaces, e.g. the ends of the precipitate in Fig. 3.

Although the Mg-K edge can be clearly seen in the EEL spectrum, the large pixel sizes used in the acquisitions and the short projected distance between Mg columns made it infeasible to distinguish individual Mg columns. The low Z contrast also made the distinction between the Mg and Al columns in HAADF–STEM images impossible. Due to these considerations, Mg elemental maps are not shown in this paper.

HAADF–STEM imaging combined with STEM–EELS mapping was used to investigate the distribution of Cu and Ag atomic columns in precipitates formed in an Al–Mg–Si–Cu–Ag alloy. Cu was found clearly localised in certain atomic columns, while Ag was spread with various occupancies in neighboring atomic columns. Most observed precipitates had regions consisting of stuctural units from the Q′ or C phases, of which we have shown two examples. Ag was seen to disrupt the formation of these ordered phases, and localize in Cu-free areas lacking repeating unit cells, which indicates that Ag forms its own local configurations inside the precipitates. While Cu was observed preferentially along coherent interfaces with the Al host lattice, Ag was localized at the narrow ends of precipitates, which have lower coherency with and induce higher strain to the host lattice. With the new possibilities of obtaining atomic-resolution compositional information from precipitate phases, the STEM–EELS technique will become an important tool for future aluminium alloy design.

This work was financially supported by The Research Council of Norway and Norsk Hydro via project no. 193619, The Norwegian–Japanese Al–Mg–Si Alloy Precipitation Project. The SuperSTEM Laboratory is the UK National Facility for Aberration-Corrected STEM, supported by the Engineering and Physical Sciences Research Council (EPSRC).

[1] H. W. Zandbergen, S. J. Andersen, J. Jansen, Science 277 (1997) 1221–1225. doi:10.1126/science.277.5330.1221.

[2] J. H. Chen, E. Costan, M. A. van Huis, Q. Xu, H. W. Zandbergen, Science 312 (2006) 416–419. doi:10.1126/science.1124199.

[3] C. D. Marioara, S. J. Andersen, T. N. Stene, H. Hasting, J. Walmsley, A. T. J. Van Helvoort, R. Holmestad, Phil. Mag. 87 (2007) 3385–3413. doi:10.1080/14786430701287377.

[4] M. Torsæter, F. J. H. Ehlers, C. D. Marioara, S. J. Andersen, R. Holmestad, Phil. Mag. 92 (2012) 3833–3856. doi:10.1080/14786435.2012.693214.

[5] L. Arnberg, B. Aurivillius, Acta Chem. Scand. 34A (1980) 1–5.

[6] C. Wolverton, Acta Materialia 49 (2001) 3129 – 3142. doi:10.1016/S1359-6454(01)00229-4.

[7] C. Ravi, C. Wolverton, Acta Materialia 52 (2004) 4213–4227. doi:10.1016/j.actamat.2004.05.037.

[8] S. Andersen, C. Marioara, R. Vissers, A. Frøseth, H. Zandbergen, Materials Science and Engineering: A 444 (2007) 157 – 169. doi:10.1016/j.msea.2006.08.084.

[9] J. Kim, C. D. Marioara, R. Holmestad, E. Kobayashi, T. Sato, Materials Science and Engineering: A 560 (2013) 154 – 162. doi:10.1016/j.msea.2012.09.051.

[10] C. D. Marioara, J. Nakamura, K. Matsuda, S. J. Andersen, R. Holmestad, T. Sato, T. Kawabata, S. Ikeno, Phil. Mag. 92 (2012) 1149–1158. doi:10.1080/14786435.2011.642319.

[11] P. D. Nellist, S. J. Pennycook, volume 113, Elsevier, 2000, pp. 147–203.

[12] T. Yamazaki, M. Kawasaki, K. Watanabe, I. Hashimoto, M. Shiojiri, Ultramicroscopy 92 (2002) 181 – 189. doi:10.1016/S0304-3991(02)00131-6.

[13] H. Rose, Ultramicroscopy 110 (2010) 488 – 499. doi:10.1016/j.ultramic.2009.10.003.

[14] P. E. Batson, N. Dellby, O. L. Krivanek, Nature 418 (2002) 617–620. doi:10.1038/nature00972.

[15] K. W. Urban, C.-L. Jia, L. Houben, M. Lentzen, S.-B. Mi, K. Tillmann, Philos. T. R. Soc. A 367 (2009) 3735–3753. doi:10.1098/rsta.2009.0134.

[16] H. Tan, S. Turner, E. Yücelen, J. Verbeeck, G. Van Tendeloo, Phys. Rev. Lett. 107 (2011) 107602. doi:10.1103/PhysRevLett.107.107602.

[17] I. MacLaren, L. Q. Wang, B. Schaffer, Q. M. Ramasse, A. J. Craven, S. M. Selbach, N. A. Spaldin, S. Miao, K. Kalantari, I. M. Reaney, Adv. Funct. Mater. 23 (2013) 683–689. doi:10.1002/adfm.201201835.

[18] A. Gubbens, M. Barfels, C. Trevor, R. Twesten, P. Mooney, P. Thomas, N. Menon, B. Kraus, C. Mao, B. McGinn, Ultramicroscopy 110 (2010) 962 – 970. doi:10.1016/j.ultramic.2010.01.009.

[19] R. Arenal, F. de la Peña, O. Stéphan, M. Walls, M. Tencé, A. Loiseau, C. Colliex, Ultramicroscopy 109 (2008) 32 – 38. doi:10.1016/j.ultramic.2008.07.005.

[20] M. D. Rossell, Q. M. Ramasse, S. D. Findlay, F. Rechberger, R. Erni, M. Niederberger, ACS Nano 6 (2012) 7077–7083. doi:10.1021/nn3021212.